JOURNAL OF THEORETICAL AND APPLIED MECHANICS
62, 2, pp. 389-401, Warsaw 2024
https://doi.org/10.15632/jtam-pl/186178

NUMERICAL MODELLING OF THE LASER HIGH-TEMPERATURE HYPERTHERMIA USING THE DUAL-PHASE LAG EQUATION[1]

Mikołaj Stryczyński, Ewa Majchrzak

Silesian University of Technology, Department of Computational Mechanics and Engineering, Gliwice, Poland
corresponding author Mikołaj Stryczyński, e-mail: mikolaj.stryczynski@polsl.pl

In the paper, thermal processes occurring in a soft tissue subjected to laser irradiation are analyzed. The bioheat transfer in an axisymmetric domain is described by a dual-phase lag equation, which takes into account temperature-dependent thermophysical parameters of the tissue. The source term in this equation is related to laser irradiation, and is determined by solving the optical diffusion equation. It is assumed that the optical parameters depend on the Arrhenius integral, which is a measure of the degree of tissue destruction. In the model, the process of evaporation of water contained in the tissue is also considered.

Keywords: bioheat transfer, hyperthermia, optical diffusion equation, dual-phase lag equation, finite difference method

1. Introduction

Oncological hyperthermia involves raising the patient's body temperature in controlled conditions. It is used to support conventional therapies, such as chemotherapy or radiotherapy. The main goal of the procedure is to induce a state of increased patient temperature, activating the immune system to eliminate cancer cells from the body. This leads to an increase in the number of leukocytes and initiates a natural intervention against the tumor (Foster *et al.*, 2020).

Thermal ablation is a procedure aimed at destroying the tumor under the influence of high temperature. Heat is delivered directly to the tumor using needles or probes, without the need to surgically open the patient's body (Barnoon and Bakhshandehfard, 2021). The procedure is often performed in combination with laparoscopic and ultrasound methods, which allow for precise localization of the tumor (Giglio *et al.*, 2020) and is performed under anesthesia to relieve pain. During thermal ablation, probes applied to the tumor are heated to a temperature ranging from 65°C to 85°C for 10 to 15 minutes. Among various heating techniques, the laser-induced hyperthermia stands out for its precision and non-invasiveness.

Destruction of cancer tissue by laser irradiation is used, among others, in removal of oncological lesions within the liver using laparoscopic methods (Ellebrecht *et al.*, 2018). This process can be modelled using a dual-phase lag equation, which includes a source component that takes into account the interaction of laser with biological tissue. To determine this component, an appropriate mathematical model that describes light propagation in biological tissues must be selected (Ashley *et al.*, 1995; Dombrovsky and Baillis, 2010; Jacques and Pogue, 2008). One of such models is the radiative transport equation but, in some cases, it is possible to approximate the radiative transport equation with the optical diffusion equation, e.g. (Dombrovsky *et al.*, 2012; Jaunich *et al.*, 2008). Considering that in soft tissues, scattering dominates over absorption for wavelengths from 650 nm to 1300 nm, the optical diffusion equation was used in this study. Many articles in the literature are devoted to modelling laser interactions with biological

[1]Paper presented during PCM-CMM 2023, Gliwice, Poland

tissues. Most of them concern the use of the Pennes equation in combination with the radiative transport equation or the optical diffusion equation, e.g. (Kim and Guo, 2007; Kim *et al.*, 1996). Papers using the dual-phase lag equation appear relatively rarely (Majchrzak *et al.*, 2019; Zhou *et al.*, 2009). Moreover, constant thermophysical and optical parameters of biological tissues are commonly assumed.

In this paper, the dual-phase lag equation combined with the optical diffusion equation is used to model the interaction of laser with biological tissues. Additionally, the temperature-dependent tissue thermophysical parameters and optical tissue parameters changing with the Arrhenius integral are taken into account.

2. Mathematical model

An axisymmetric fragment of the liver subjected to laser irradiation is considered, as shown in Fig. 1. The dual–phase lag equation is based on the following relationship between the heat flux and temperature gradient (Tzou, 1995)

$$\mathbf{q}(r,z,t+\tau_q) = -\lambda(T)\,\mathrm{grad}\,T(r,z,t+\tau_T) \tag{2.1}$$

where τ_q represents the delay in the appearance of heat flux and its associated conduction through the medium, τ_T is the delay in the appearance of temperature gradient caused by heat conduction through structures of a small scale or size, λ is the thermal conductivity coefficient, T denotes temperature, $\mathbf{q}$ is the heat flux, r, z represent geometrical coordinates, and t is a time. This relationship is called generalized Fourier's law, because for time delays equal to zero ($\tau_T = \tau_q = 0$), one obtains the classical Fourier law.

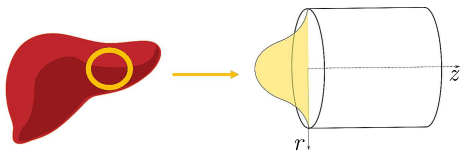

Fig. 1. An axisymmetric fragment of the liver

The functions $T(r,z,t+\tau_T)$ and $\mathbf{q}(r,z,t+\tau_q)$ are expanded into a Taylor series with an accuracy to the first derivatives

$$\mathbf{q}(r,z,t) + \tau_q \frac{\partial \mathbf{q}(r,z,t)}{\partial t} = \lambda(T)\,\mathrm{grad}\,T(r,z,t) + \tau_T \lambda(T) \frac{\partial[\,\mathrm{grad}\,T(r,z,t)]}{\partial t} \tag{2.2}$$

As known, the Fourier equation has the following form

$$c(T)\rho(T)\frac{\partial T(r,z,t)}{\partial t} = -\,\mathrm{div}\,\mathbf{q}(r,z,t) + Q(r,z,t) \tag{2.3}$$

where $c(T)$ is the specific heat of tissue, $\rho(T)$ is mass density and $Q(r,z,t)$ is the source function.

Basing on Eqs. (2.2) and (2.3), after appropriate transformations, the final form of the dual-phase lag is obtained (the arguments are omitted for simplicity) (Majchrzak and Stryczyński, 2022)

$$C(T)\frac{\partial T}{\partial t} + \tau_q \frac{\partial}{\partial t}\left[C(T)\frac{\partial T}{\partial t}\right] = \mathrm{div}\,[\lambda(T)\,\mathrm{grad}\,T] + \tau_T\,\mathrm{div}\left[\lambda(T)\frac{\partial(\,\mathrm{grad}\,T)}{\partial t}\right] + Q + \tau_q \frac{\partial Q}{\partial t} \tag{2.4}$$

where $C(T) = c(T)\rho(T)$ is the volumetric thermal capacity, and

$$Q = w(\psi)c_b(T_a - T) + Q_{met}(\psi) + Q_{ext} \tag{2.5}$$

while $w(\psi)$ is the blood perfusion rate, c_b is the specific heat of blood, T_a is the arterial temperature, $Q_{met}(\psi)$ is the metabolic heat source. Q_{ext} is the source function related to laser irradiation, and ψ is the so-called Arrhenius integral (Niemz, 2007)

$$\psi = \psi(r,z,t^f) = P\int_0^{t^f} \exp\Big(-\frac{E}{RT(r,z,t)}\Big)\,dt \tag{2.6}$$

where P is the pre-exponential factor, E is the activation energy, R is the universal gas constant, and $[0,t^f]$ is the time interval under consideration.

It should be emphasized that the calculation of the Arrhenius integral allows us to estimate the degree of destruction of biological tissue. Thus, a value of damage integral $\psi(r,z,t^f)=1$ corresponds to a 63% probability of cell death at a specific point (r,z), while $\psi(r,z,t^f)=4.6$ corresponds to 99% probability of cell death at this point. The value $\psi(r,z,t^f)=1$ is treated as extremely important because, from this moment, the tissue coagulation begins (Niemz, 2007).

Because

$$\frac{\partial}{\partial t}\Big[C(T)\frac{\partial T}{\partial t}\Big] = \frac{\partial C(T)}{\partial t}\frac{\partial T}{\partial t} + C(T)\frac{\partial^2 T}{\partial t^2} = \frac{dC(T)}{dT}\Big(\frac{\partial T}{\partial t}\Big)^2 + C(T)\frac{\partial^2 T}{\partial t^2} \tag{2.7}$$

thus Eq. (2.4) can be written in the form

$$\begin{aligned} &C(T)\Big(\frac{\partial T}{\partial t} + \tau_q\frac{\partial^2 T}{\partial t^2}\Big) + \tau_q\frac{dC(T)}{dT}\Big(\frac{\partial T}{\partial t}\Big)^2 \\ &\quad = \operatorname{div}\Big[\lambda(T)\operatorname{grad}T\Big] + \tau_T\operatorname{div}\Big[\lambda(T)\frac{\partial(\operatorname{grad}T)}{\partial t}\Big] + Q + \tau_q\frac{\partial Q}{\partial t} \end{aligned} \tag{2.8}$$

When the biological tissue reaches a temperature of approximately 100°C then in the mathematical model of the heating process, the phenomenon of water evaporation within the tissue should be taken into account. In this case, an additional source term related to the evaporation is introduced. This term is denoted as $Q_{evap}(T)$, and takes the following form (Yang *et al.*, 2007; Mochnacki and Majchrzak, 2007)

$$Q_{evap}(T) = L\frac{\partial W}{\partial t} = L\frac{dW}{dT}\frac{\partial T}{\partial t} \tag{2.9}$$

where L is the latent heat of water vaporization and W is the water volumetric fraction in the tissue domain. Thus

$$Q_{evap}(T) + \tau_q\frac{\partial Q_{evap}(T)}{\partial t} = L\frac{dW}{dT}\frac{\partial T}{\partial t} + \tau_q L\Big[\frac{d^2W}{dT^2}\Big(\frac{\partial T}{\partial t}\Big)^2 + \frac{dW}{dT}\frac{\partial^2 T}{\partial t^2}\Big] \tag{2.10}$$

Introducing dependence (2.10) into the dual-phase lag equation (2.8), one obtains

$$\begin{aligned} &\Big[C(T) - L\frac{dW}{dT}\Big]\frac{\partial T}{\partial t} + \tau_q\Big[C(T) - L\frac{dW}{dT}\Big]\frac{\partial^2 T}{\partial t^2} + \tau_q\Big[\frac{dC(T)}{dT} - L\frac{d^2W}{dT^2}\Big]\Big(\frac{\partial T}{\partial t}\Big)^2 \\ &\quad = \operatorname{div}\Big[\lambda(T)\operatorname{grad}T\Big] + \tau_T\operatorname{div}\Big[\lambda(T)\frac{\partial(\operatorname{grad}T)}{\partial t}\Big] + Q + \tau_q\frac{\partial Q}{\partial t} \end{aligned} \tag{2.11}$$

or

$$\begin{aligned} &\widehat{C}(T)\Big(\frac{\partial T}{\partial t} + \tau_q\frac{\partial^2 T}{\partial t^2}\Big) + \tau_q\frac{d\widehat{C}(T)}{dT}\Big(\frac{\partial T}{\partial t}\Big)^2 \\ &\quad = \operatorname{div}\Big[\lambda(T)\operatorname{grad}T\Big] + \tau_T\operatorname{div}\Big[\lambda(T)\frac{\partial(\operatorname{grad}T)}{\partial t}\Big] + Q + \tau_q\frac{\partial Q}{\partial t} \end{aligned} \tag{2.12}$$

where

$$\widehat{C} = C(T) - L\frac{dW}{dT} \tag{2.13}$$

is the effective volumetric specific heat (substitute thermal capacity).

Equation (2.12) is supplemented by boundary condition (Majchrzak and Stryczyński, 2022)

$$(r,z) \in \Gamma \cup \Gamma_0 : \qquad -\lambda(T)\Big(\mathbf{n}\cdot \operatorname{grad} T + \tau_T \mathbf{n}\cdot \operatorname{grad}\frac{\partial T}{\partial t}\Big) = 0 \tag{2.14}$$

where $\mathbf{n}$ is the normal outward vector, Γ_0 is the axis of the cylinder, and Γ is the outer surface of the cylinder.

The initial conditions are also known

$$t = 0 \qquad T = T_p \qquad \frac{\partial T}{\partial t} = \frac{Q(T_p)}{\widehat{C}(T_p)} \tag{2.15}$$

where T_p is the initial temperature of tissue.

As mentioned earlier, in soft tissues, the scattering dominates over absorption for wavelengths from 650 to 1300 nm, and then the source function Q_{ext} related to laser irradiation appearing in Eq. (2.12) (c.f. formula (2.5)) is of the form (Jasiński *et al.*, 2016)

$$Q_{ext}(r,z,t) = \mu_a \phi(r,z) p(t) \tag{2.16}$$

where μ_a is the absorption coefficient, $\phi(r,z)$ is the total light fluence rate and $p(t)$ is the function equal to 1 when laser is *on* and equal to 0 when laser is *off*.

The total light fluence $\phi(r,z)$ is the sum of collimated part $\phi(r,z)$ and diffuse part $\phi_d(r,z)$ (Abraham and Sparrow, 2007; Jasiński *et al.*, 2016)

$$\phi(r,z) = \phi_c(r,z) + \phi_d(r,z) \tag{2.17}$$

In the case of soft tissues, in order to determine the diffuse fluence rate, the steady-state optical diffusion equation (Dombrovsky *et al.*, 2012; Kim *et al.*, 2007) should be solved

$$(r,z) \in \Omega : \qquad \operatorname{div}[D \operatorname{grad}\phi_d(r,z)] - \mu_a \phi_d(r,z) + \mu_s' \phi_c(r,z) = 0 \tag{2.18}$$

where

$$D = \frac{1}{3[\mu_a + (1-g)\mu_s]} \tag{2.19}$$

and $\mu_s' = (1-g)\mu_s$ is the effective scattering coefficient (μ_s is the scattering coefficient, g is the anisotropy factor).

Equation (2.18) is supplemented by the boundary conditions

$$-D\mathbf{n}\cdot \operatorname{grad}\phi_d(r,z) = \begin{cases} \dfrac{\phi_d(r,z)}{2} & \text{for} \quad (r,z) \in \Gamma \\ 0 & \text{for} \quad (r,z) \in \Gamma_0 \end{cases} \tag{2.20}$$

The collimated fluence rate is given as (Zhou *et al.*, 2009)

$$\phi_c(r,z) = I_0 \exp(-\mu_t' z) \exp\Big(-\frac{r^2}{r_D^2}\Big) \tag{2.21}$$

where I_0 is the surface irradiance of laser, r_D is the radius of laser beam, and μ_t' is the attenuation coefficient defined as

$$\mu_t' = \mu_a + \mu_s' \tag{2.22}$$

It should be pointed out that the optical parameters depend on the degree of tissue damage described by the Arrhenius integral, and take the form (Fasano *et al.*, 2010)

$$\begin{aligned}
\mu_a &= \mu_a(\psi) = \exp(-\psi)\mu_{a,n} + [1-\exp(-\psi)]\mu_{a,c} \\
\mu_s &= \mu_s(\psi) = \exp(-\psi)\mu_{s,n} + [1-\exp(-\psi)]\mu_{s,c} \\
g &= g(\psi) = \exp(-\psi)g_n + [1-\exp(-\psi)]g_c
\end{aligned} \tag{2.23}$$

where the indexes n and c represent the tissue in its natural and coagulated state.

Summing up, at first, equation (2.18) supplemented by boundary conditions (2.20) and next dual-phase lag equation (2.12) with boundary condition (2.14) and initial conditions (2.15), should be solved.

3. Method of solution

First, optical diffusion equation (2.18) is considered. For a cylindrical co-ordinate system, we have

$$\operatorname{div}(D\operatorname{grad}) = \frac{1}{r}\frac{\partial}{\partial r}\Big(rD\frac{\partial\phi_d}{\partial r}\Big) + \frac{\partial}{\partial z}\Big(D\frac{\partial\phi_d}{\partial z}\Big) \tag{3.1}$$

After determining the appropriate derivatives, one obtains

$$\operatorname{div}(D\operatorname{grad}) = \frac{1}{r}D\frac{\partial\phi_d}{\partial r} + D\Big(\frac{\partial^2\phi_d}{\partial r^2} + \frac{\partial^2\phi_d}{\partial z^2}\Big) + \frac{\partial D}{\partial r}\frac{\partial\phi_d}{\partial r} + \frac{\partial D}{\partial z}\frac{\partial\phi_d}{\partial z} \tag{3.2}$$

Since the diffusion coefficient D (Eq. (2.19)) depends on the parameters μ_a, μ_s and g, the parameters μ_a, μ_s, g depend on the Arrhenius integral (Eq. (2.23)), and the Arrhenius integral depends on temperature (Eq. (2.6)), the derivatives $\partial D/\partial r$ and $\partial D/\partial z$ are calculated using the chain rule

$$\begin{aligned}
\frac{\partial D}{\partial r} &= \frac{\partial D}{\partial\mu_a}\frac{\partial\mu_a}{\partial\psi}\frac{\partial\psi}{\partial T}\frac{\partial T}{\partial r} + \frac{\partial D}{\partial\mu_s}\frac{\partial\mu_s}{\partial\psi}\frac{\partial\psi}{\partial T}\frac{\partial T}{\partial r} + \frac{\partial D}{\partial g}\frac{\partial g}{\partial\psi}\frac{\partial\psi}{\partial T}\frac{\partial T}{\partial r} \\
&= \Big(\frac{\partial D}{\partial\mu_a}\frac{\partial\mu_a}{\partial\psi} + \frac{\partial D}{\partial\mu_s}\frac{\partial\mu_s}{\partial\psi} + \frac{\partial D}{\partial g}\frac{\partial g}{\partial\psi}\Big)\frac{\partial\psi}{\partial T}\frac{\partial T}{\partial r} = P\frac{\partial T}{\partial r}
\end{aligned} \tag{3.3}$$

and

$$\frac{\partial D}{\partial z} = \Big(\frac{\partial D}{\partial\mu_a}\frac{\partial\mu_a}{\partial\psi} + \frac{\partial D}{\partial\mu_s}\frac{\partial\mu_s}{\partial\psi} + \frac{\partial D}{\partial g}\frac{\partial g}{\partial\psi}\Big)\frac{\partial\psi}{\partial T}\frac{\partial T}{\partial z} = P\frac{\partial T}{\partial z} \tag{3.4}$$

where

$$P = \Big(\frac{\partial D}{\partial\mu_a}\frac{\partial\mu_a}{\partial\psi} + \frac{\partial D}{\partial\mu_s}\frac{\partial\mu_s}{\partial\psi} + \frac{\partial D}{\partial g}\frac{\partial g}{\partial\psi}\Big)\frac{\partial\psi}{\partial T} \tag{3.5}$$

Finally, Eq. (2.18) can be written in the form

$$\frac{1}{r}D\frac{\partial\phi_d}{\partial r} + D\Big(\frac{\partial^2\phi_d}{\partial r^2} + \frac{\partial^2\phi_d}{\partial z^2}\Big) + P\Big(\frac{\partial T}{\partial r}\frac{\partial\phi_d}{\partial r} + \frac{\partial T}{\partial z}\frac{\partial\phi_d}{\partial z}\Big) - \mu_a\phi_d + \mu_s'\phi_c = 0 \tag{3.6}$$

Optical diffusion equation (3.6) is solved using the finite difference method (FDM). The differential grid is shown in Fig. 2. For the internal nodes (i,j), where $i = 1,2,\ldots,m-1$ and $j = 1,2,\ldots,n-1$, the following FDM approximation of this equation is proposed

$$\begin{aligned}
&\frac{1}{r_{i,j}}D^f_{i,j}\frac{\phi^f_{d,i+1,j} - \phi^f_{d,i-1,j}}{2h} + D^f_{i,j}\frac{\phi^f_{d,i-1,j} - 2\phi^f_{d,i,j} + \phi^f_{d,i+1,j}}{h^2} \\
&\quad + D^f_{i,j}\frac{\phi^f_{d,i,j-1} - 2\phi^f_{d,i,j} + \phi^f_{d,i,j+1}}{h^2} + P_{i,j}\frac{T^f_{i+1,j} - T^f_{i-1,j}}{2h}\frac{\phi^f_{d,i+1,j} - \phi^f_{d,i-1,j}}{2h} \\
&\quad + P_{i,j}\frac{T^f_{i,j+1} - T^f_{i,j-1}}{2h}\frac{\phi^f_{d,i,j+1} - \phi^f_{d,i,j-1}}{2h} - \mu^f_{a,i,j}\phi^f_{d,i,j} + \mu'^f_{s,i,j}\phi_{c,i,j} = 0
\end{aligned} \tag{3.7}$$

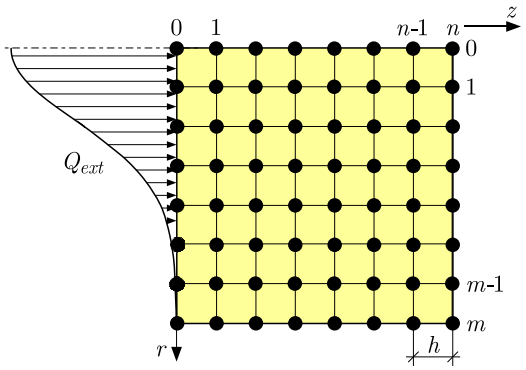

Fig. 2. Differential mesh

or

$$\phi^f_{d,i,j} = \frac{1}{r_{i,j}} D^f_{i,j} \frac{\phi^f_{d,i+1,j} - \phi^f_{d,i-1,j}}{2hG^f_{i,j}} + D^f_{i,j} \frac{\phi^f_{d,i-1,j} + \phi^f_{d,i+1,j} + \phi^f_{d,i,j-1} + \phi^f_{d,i,j+1}}{h^2 G^f_{i,j}}$$
$$+ P^f_{i,j} \frac{T^f_{i+1,j} - T^f_{i-1,j}}{2hG^f_{i,j}} \frac{\phi^f_{d,i+1,j} - \phi^f_{d,i-1,j}}{2h} \tag{3.8}$$
$$+ P^f_{i,j} \frac{T^f_{i,j+1} - T^f_{i,j-1}}{2hG^f_{i,j}} \frac{\phi^f_{d,i+1,j} - \phi^f_{d,i-1,j}}{2h} + \frac{\mu'^f_{s,i,j}}{G^f_{i,j}} \phi_{c,i,j}$$

where

$$G^f_{i,j} = 4\frac{D^f_{i,j}}{h^2} + \mu^f_{a,i,j} \tag{3.9}$$

Boundary conditions (2.20) are approximated in a similar way, and then:
— for $j = 0$, $i = 1, 2, \ldots, m-1$

$$\phi^f_{d,i,j} = \frac{2D^f_{i,j}}{2D^f_{i,j} + h} \phi^f_{d,i,j+1} \tag{3.10}$$

— for $j = n$, $i = 1, 2, \ldots, m-1$

$$\phi^f_{d,i,j} = \frac{2D^f_{i,j}}{2D^f_{i,j} + h} \phi^f_{d,i,j-1} \tag{3.11}$$

— for $i = 0$, $j = 1, 2, \ldots, n-1$

$$\phi^f_{d,i,j} = \phi^f_{d,i+1,j} \tag{3.12}$$

— for $i = m$, $j = 1, 2, \ldots, n-1$

$$\phi^f_{d,i,j} = \frac{2D^f_{i,j}}{2D^f_{i,j} + h} \phi^f_{d,i-1,j} \tag{3.13}$$

It should be pointed out that the f index means that the optical diffusion equation due to variable optical parameters must be solved at each time step. To summarize the algorithm, at each time step, the values of optical parameters dependent on the Arrhenius integral (Eqs. (2.23)) are calculated. The collimated part of the light fluence is determined (Eq. (2.21)) and the diffuse

part is determined by solving the system of Eqs. (3.8)-(3.13). This system was solved using the iterative Gaussian method. Then, the source component Q_{ext} is calculated from formula (2.16).

Now, the method of solving the dual-phase lag equation will be presented. Equation (2.12) can be written in the form (c.f. formula (2.5))

$$\begin{aligned}\widehat{C}(T)\Big(\frac{\partial T}{\partial t}+\tau_q\frac{\partial^2 T}{\partial t^2}\Big)+\tau_q\frac{d\widehat{C}(T)}{dT}\Big(\frac{\partial T}{\partial t}\Big)^2 &= \operatorname{div}\Big[\lambda(T)\operatorname{grad}T\Big]\\ &+\tau_T\operatorname{div}\Big[\lambda(T)\frac{\partial(\operatorname{grad}T)}{\partial t}\Big]+w(\psi)c_b(T_a-T)+Q_{met}(\psi)+Q_{ext}\\ &+\tau_q\Big(\frac{dw(\psi)}{d\psi}\frac{\partial\psi}{\partial t}c_b(T_a-T)-w(\psi)c_b\frac{\partial T}{\partial t}+\frac{dQ_{met}(\psi)}{d\psi}\frac{\partial\psi}{\partial t}+\frac{\partial Q_{ext}}{\partial t}\Big)\end{aligned} \tag{3.14}$$

or

$$\begin{aligned}&[\widehat{C}(T)+\tau_q w(\psi)c_b]\frac{\partial T}{\partial t}+\tau_q\widehat{C}(T)\frac{\partial^2 T}{\partial t^2}+\tau_q\frac{d\widehat{C}(T)}{dT}\Big(\frac{\partial T}{\partial t}\Big)^2\\ &\quad=\operatorname{div}[\lambda(T)\operatorname{grad}T]+\tau_T\operatorname{div}\Big[\lambda(T)\frac{\partial(\operatorname{grad}T)}{\partial t}\Big]+w(\psi)c_b(T_a-T)\\ &\quad+Q_{met}(\psi)+Q_{ext}+\tau_q\Big(\frac{dw(\psi)}{d\psi}\frac{\partial\psi}{\partial t}c_b(T_a-T)+\frac{dQ_{met}(\psi)}{d\psi}\frac{\partial\psi}{\partial t}+\frac{\partial Q_{ext}}{\partial t}\Big)\end{aligned} \tag{3.15}$$

where (Majchrzak and Stryczyński, 2022)

$$\begin{aligned}&\operatorname{div}[\lambda(T)\operatorname{grad}T]+\tau_T\operatorname{div}\Big[\lambda(T)\operatorname{grad}\frac{\partial T}{\partial t}\Big]=\frac{1}{r}\lambda(T)\Big[\frac{\partial T}{\partial r}+\tau_T\frac{\partial}{\partial r}\Big(\frac{\partial T}{\partial t}\Big)\Big]\\ &+\frac{d\lambda(T)}{dT}\frac{\partial T}{\partial r}\Big[\frac{\partial T}{\partial r}+\tau_T\frac{\partial}{\partial r}\Big(\frac{\partial T}{\partial t}\Big)\Big]+\lambda(T)\Big[\frac{\partial^2 T}{\partial r^2}+\tau_T\frac{\partial^2}{\partial r^2}\Big(\frac{\partial T}{\partial t}\Big)\Big]\\ &+\frac{d\lambda(T)}{dT}\frac{\partial T}{\partial z}\Big[\frac{\partial T}{\partial z}+\tau_T\frac{\partial}{\partial z}\Big(\frac{\partial T}{\partial t}\Big)\Big]+\lambda(T)\Big[\frac{\partial^2 T}{\partial z^2}+\tau_T\frac{\partial^2}{\partial z^2}\Big(\frac{\partial T}{\partial t}\Big)\Big]\end{aligned} \tag{3.16}$$

To solve Eq. (3.15), the implicit scheme of the finite difference method is used. For internal node (i,j), $i=1,2,\ldots,m-1$, $j=1,2,\ldots,n-1$ and transition $t^f\to t^{f+1}$, the following approximation of operator (3.16) is obtained (Majchrzak and Stryczyński, 2022)

$$\begin{aligned}&\operatorname{div}[\lambda(T)\operatorname{grad}T]_{i,j}^{f+1}+\tau_T\operatorname{div}\Big[\lambda(T)\operatorname{grad}\frac{\partial T}{\partial t}\Big]_{i,j}^{f+1}=A_{i,j}^f\Big(1-\frac{h}{2r_{i,j}}\Big)T_{i-1,j}^{f+1}\\ &+A_{i,j}^f\Big(1+\frac{h}{2r_{i,j}}\Big)T_{i+1,j}^{f+1}+A_{i,j}^f(T_{i,j-1}^{f+1}+T_{i,j+1}^{f+1})-4A_{i,j}^f T_{i,j}^{f+1}+B_{i,j}^f\end{aligned} \tag{3.17}$$

where

$$A_{i,j}^f=\frac{\lambda_{i,j}^f(\Delta t+\tau_T)}{h^2\Delta t} \tag{3.18}$$

and

$$\begin{aligned}B_{i,j}^f&=-\frac{\lambda_{i,j}^f\tau_T}{h^2\Delta t}(T_{i-1,j}^f+T_{i+1,j}^f+T_{i,j-1}^f+T_{i,j+1}^f-4T_{i,j}^f)-\frac{\lambda_{i,j}^f\tau_T}{2hr_{i,j}\Delta t}(T_{i+1,j}^f-T_{i-1,j}^f)\\ &+\frac{1}{4h^2\Delta t}\Big(\frac{d\lambda(T)}{dT}\Big)_{i,j}^f[(\Delta t+\tau_T)(T_{i+1,j}^f-T_{i-1,j}^f)^2-\tau_T(T_{i+1,j}^f-T_{i-1,j}^f)(T_{i+1,j}^{f-1}-T_{i-1,j}^{f-1})]\\ &+\frac{1}{4h^2\Delta t}\Big(\frac{d\lambda(T)}{dT}\Big)_{i,j}^f[(\Delta t+\tau_T)(T_{i,j+1}^f-T_{i,j-1}^f)^2-\tau_T(T_{i,j+1}^f-T_{i,j-1}^f)(T_{i,j+1}^{f-1}-T_{i,j-1}^{f-1})]\end{aligned} \tag{3.19}$$

while Δt is the time step.

The approximation of the left-hand side of Eq. (3.15) is the following

$$\begin{aligned}&\Big\{[\widehat{C}(T)+\tau_q w(\psi)c_b]\frac{\partial T}{\partial t}+\tau_q\widehat{C}(T)\frac{\partial^2 T}{\partial t^2}+\tau_q\frac{d\widehat{C}(T)}{dT}\Big(\frac{\partial T}{\partial t}\Big)^2\Big\}_{i,j}^{f+1}\\&\quad=(\widehat{C}_{i,j}^f+w_{i,j}^f c_b)\frac{T_{i,j}^{f+1}-T_{i,j}^f}{\Delta t}+\tau_q\widehat{C}_{i,j}^f\frac{T_{i,j}^{f+1}-2T_{i,j}^f+T_{i,j}^{f-1}}{(\Delta t)^2}\\&\quad+\tau_q\Big(\frac{d\widehat{C}(T)}{dT}\Big)_{i,j}^f\Big(\frac{T_{i,j}^f-T_{i,j}^{f-1}}{\Delta t}\Big)^2\end{aligned}\tag{3.20}$$

Thus, one obtains finally the approximation of Eq. (3.15) in the form

$$\begin{aligned}&(\widehat{C}_{i,j}^f+\tau_q w_{i,j}^f c_b)\frac{T_{i,j}^{f+1}-T_{i,j}^f}{\Delta t}+\tau_q\widehat{C}_{i,j}^f\frac{T_{i,j}^{f+1}-2T_{i,j}^f+T_{i,j}^{f-1}}{(\Delta t)^2}\\&\quad+\tau_q\Big(\frac{d\widehat{C}(T)}{dT}\Big)_{i,j}^f\Big(\frac{T_{i,j}^f-T_{i,j}^{f-1}}{\Delta t}\Big)^2=A_{i,j}^f\Big(1-\frac{h}{2r_{i,j}}\Big)T_{i-1,j}^{f+1}+A_{i,j}^f\Big(1+\frac{h}{2r_{i,j}}\Big)T_{i+1,j}^{f+1}\\&\quad+A_{i,j}^f(T_{i,j-1}^{f+1}+T_{i,j+1}^{f+1})-4A_{i,j}^f T_{i,j}^{f+1}-c_b\Big[w_{i,j}^f+\tau_q\Big(\frac{dw(\psi)}{d\psi}\frac{\partial\psi}{\partial t}\Big)_{i,j}^f\Big]T_{i,j}^{f+1}+D_{i,j}^f\end{aligned}\tag{3.21}$$

where

$$\begin{aligned}D_{i,j}^f&=B_{i,j}^f+w_{i,j}^f c_b T_a+(Q_{met})_{i,j}^f+(Q_{ext})_{i,j}^f\\&\quad+\tau_q\Big[\Big(\frac{dw(\psi)}{d\psi}\frac{\partial\psi}{\partial t}\Big)_{i,j}^f c_b T_a+\Big(\frac{dQ_{met}(\psi)}{d\psi}\frac{\partial\psi}{\partial t}\Big)_{i,j}^f+\Big(\frac{\partial Q_{ext}}{\partial t}\Big)_{i,j}^f\Big]\end{aligned}\tag{3.22}$$

From Eq. (3.21), it results

$$T_{i,j}^{f+1}=\frac{A_{i,j}^f}{F_{i,j}^f}\Big(1-\frac{h}{2r_{i,j}}\Big)T_{i-1,j}^{f+1}+\frac{A_{i,j}^f}{F_{i,j}^f}\Big(1+\frac{h}{2r_{i,j}}\Big)T_{i+1,j}^{f+1}+\frac{A_{i,j}^f}{F_{i,j}^f}(T_{i,j-1}^{f+1}+T_{i,j+1}^{f+1})+\frac{E_{i,j}^f}{F_{i,j}^f}\tag{3.23}$$

where

$$E_{i,j}^f=D_{i,j}^f+\frac{(\widehat{C}_{i,j}^f+\tau_q w_{i,j}^f c_b)\Delta t+2\tau_q\widehat{C}_{i,j}^f}{(\Delta t)^2}T_{i,j}^f-\frac{\widehat{C}_{i,j}^f\tau_q}{(\Delta t)^2}T_{i,j}^{f-1}-\tau_q\Big(\frac{d\widehat{C}(T)}{dT}\Big)_{i,j}^f\Big(\frac{T_{i,j}^f-T_{i,j}^{f-1}}{\Delta t}\Big)^2\tag{3.24}$$

$$F_{i,j}^f=\frac{(\widehat{C}_{i,j}^f+\tau_q w_{i,j}^f c_b)\Delta t+\tau_q\widehat{C}_{i,j}^f}{(\Delta t)^2}+4A_{i,j}^f+c_b\Big[w_{i,j}^f+\tau_q\Big(\frac{dw(\psi)}{d\psi}\frac{\partial\psi}{\partial t}\Big)_{i,j}^f\Big]$$

Boundary condition (2.14) should also be approximated (Majchrzak and Stryczyński, 2022).

At each time step, the system of equations (3.23) is solved using the Gauss-Seidl iterative method.

4. Results of computations

An axisymmetric fragment of the biological tissue (liver) of dimensions $R = 0.02\,\mathrm{m}$ and $Z = 0.02\,\mathrm{m}$ is considered (Fig. 2).

To solve modified dual-phase lag Eq. (2.12), the temperature dependence of water content is needed. Based upon experiments that the measured water content as a function of temperature, the following dependence is used (Yang *et al.*, 2007)

$$W(T)=0.778\begin{cases}1-\exp\Big(\dfrac{T-106}{3.42}\Big) & \text{for} \quad T\leqslant 103^\circ\mathrm{C}\\ S(T) & \text{for} \quad 103^\circ\mathrm{C}\leqslant T\leqslant 104^\circ\mathrm{C}\\ \exp\Big(\dfrac{-(T-80)}{34.37}\Big) & \text{for} \quad T\geqslant 104^\circ\mathrm{C}\end{cases}\tag{4.1}$$

where $S(T)$ is a cubic C^1 spline between two exponential functions, and has the following form

$$S(T) = -4.05821416 \cdot 10^4 + 1.18204602 \cdot 10^3 T - 11.4752357 T^2 + 3.71298243 \cdot 10^{-2} T^3 \quad (4.2)$$

In Fig. 3, the course of function $W(T)$ is shown. As can be seen, the water content of the soft tissue is approximately 77.8% by volume and remains almost constant until the phase transition temperature is reached. As the temperature increases further, the water content gradually decreases down to approximately 20% of the volume at 130°C.

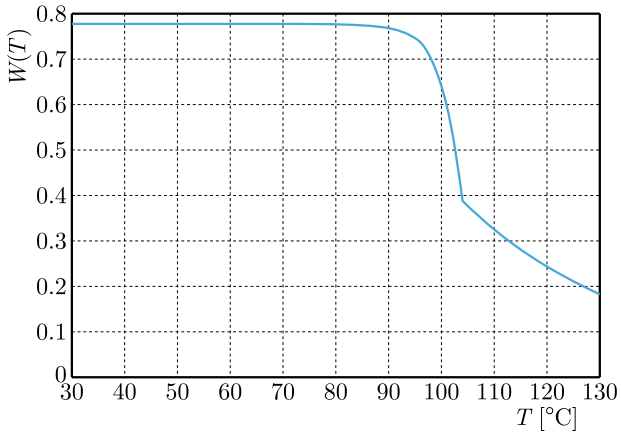

Fig. 3. The water content in soft tissue as a function of temperature

The temperature-dependent thermal conductivity and volumetric specific heat of the liver tissue are taken from Lopresto *et al.* (2019)

$$\lambda(T) = \begin{cases} 0.5075 + 5.6261 \cdot 10^{-51} T^{25.296} & \text{for} \quad T \leqslant 99^\circ\text{C} \\ S_\lambda(T) & \text{for} \quad 99^\circ\text{C} \leqslant T \leqslant 101^\circ\text{C} \\ 55.44 - 0.99701 T + 4.4988 \cdot 10^{-3} T^2 & \text{for} \quad T \geqslant 101^\circ\text{C} \end{cases}$$

$$C(T) = \begin{cases} 3.3012 + \dfrac{3.6186}{100 - T} & \text{for} \quad T \leqslant 99^\circ\text{C} \\ S_C(T) & \text{for} \quad 99^\circ\text{C} \leqslant T \leqslant 101^\circ\text{C} \\ 90.808 - 1.5491 T + 6.6664 \cdot 10^{-3} T^2 & \text{for} \quad T \geqslant 101^\circ\text{C} \end{cases} \quad (4.3)$$

where $S_\lambda(T)$ and $S_C(T)$ are the cubic C^1 splines.

Tissue destruction significantly affects the blood flow process. Abraham and Sparrow (2007) presented the following relationship between the blood perfusion rate and the degree of tissue damage

$$w(\psi) = \begin{cases} (1 + 25\psi - 260\psi^2) w_{b0} & \text{for} \quad 0 \leqslant \psi \leqslant 0.1 \\ (1 - \psi) w_{b0} & \text{for} \quad 0.1 \leqslant \psi \leqslant 1 \\ 0 & \text{for} \quad \psi \geqslant 1 \end{cases} \quad (4.4)$$

where $w_{b0} = 0.5\,\text{kg}/(\text{m}^3\text{s})$ is the baseline value of the blood perfusion rate.

A similar relationship is assumed for the metabolic term (Abraham and Sparrow, 2007)

$$Q_{met}(\psi) = \begin{cases} (1 + 25\psi - 260\psi^2) Q_{m0} & \text{for} \quad 0 \leqslant \psi \leqslant 0.1 \\ (1 - \psi) Q_{m0} & \text{for} \quad 0.1 \leqslant \psi \leqslant 1 \\ 0 & \text{for} \quad \psi \geqslant 1 \end{cases} \quad (4.5)$$

where $Q_{m0} = 245\,\text{W}/\text{m}^3$ is the baseline value of the metabolic heat source.

The remaining data used at the stage of numerical computations are collected below: initial temperature $T_p = 37°\text{C}$, relaxation time $\tau_q = 4\,\text{s}$, thermalization time $\tau_T = 2\,\text{s}$, optical parameters: $\mu_{a,n} = 195\,1/\text{m}$, $\mu_{a,c} = 13\,1/\text{m}$, $\mu_{s,n} = 4350\,1/\text{m}$, $\mu_{s,c} = 30590\,1/\text{m}$, $g_n = 0.0931$ and $g_c = 0.09165$ (Fasano *et al.*, 2010), specific heat of blood $c_b = 3770\,\text{J/(kgK)}$, arterial temperature $T_a = 37°\text{C}$, radius of laser beam $r_D = 0.001\,\text{m}$. In the Arrhenius integral (2.6): $P = 7.39{\cdot}10^{37}\,1/\text{s}$, $E = 2.58 \cdot 10^5\,\text{J/mol}$, $R = 8.314\,\text{J/(mol K)}$ (Szasz *et al.*, 2011).

The computations were performed for the difference mesh $m = n = 100$ nodes using the time step $\Delta t = 0.0005\,\text{s}$ until reaching the observation time, which was set to 150 seconds.

Before proceeding to the detailed analysis, calculations were performed for both constant and Arrhenius integral-dependent optical parameters in order to investigate the difference in temperature profiles. It was assumed that the laser operated for 120 s with power $I_0 = 1.33 \cdot 10^5\,\text{W/m}^2$.

A comparison of the results for constant and variable optical parameters is shown in Fig. 4 in the form of temperature profiles at the point with coordinates $(0.0002\,\text{m}, 0.0002\,\text{m})$. As can be seen, in the case of variable optical parameters, a much lower temperature was achieved. This is due to significant changes in the values of tissue scattering and absorption coefficients in the coagulated and natural state. The temperature difference is significant. It can, therefore, be concluded that in the case of high-temperature hyperthermia, it is important to take into account the optical parameters of the tissue that change with the Arrhenius integral. Otherwise, overestimated temperatures may be obtained, which may lead to incorrect predictions of tissue damage.

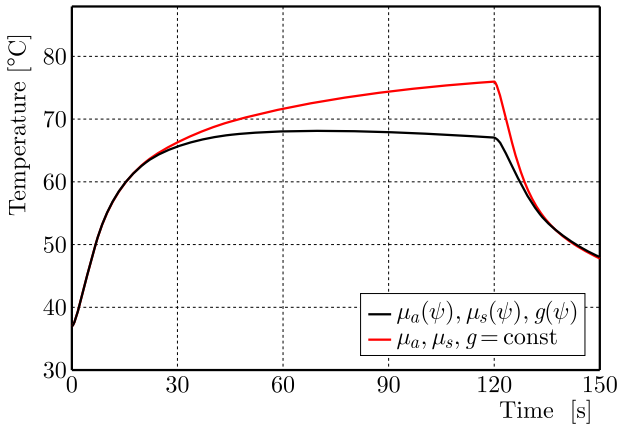

Fig. 4. Temperature history for constant and variable optical parameters, $I_0 = 1.33 \cdot 10^5\,\text{W/m}^2$, exposure time 120 s – point $(0.0002\,\text{m}, 0.0002\,\text{m})$

Then, calculations were performed for three different laser irradiation powers: $I_0 = 1.33 \cdot 10^5\,\text{W/m}^2$, $I_0 = 2 \cdot 10^5\,\text{W/m}^2$ and $I_0 = 2.5 \cdot 10^5\,\text{W/m}^2$ with an exposure time of 120 s. The temperature profiles marked with a dashed line in Fig. 5 correspond to the model using the function $W(T)$, while the solid line refers to the model without the function taking into account the percentage of water content in the tissue. As observed, at low laser powers, there are no significant differences between the obtained temperatures. However, the discrepancies increase as I_0 increases. The greatest differences occur at the moment when the maximum temperature is reached. Taking into account the process of water evaporation gives lower temperatures, which is related to the release of the latent heat of evaporation of water. In later stages of the process, the temperature profiles become equal again.

Further computations were carried out for higher laser powers, namely: $I_0 = 5 \cdot 10^5\,\text{W/m}^2$, $I_0 = 10{\cdot}10^5\,\text{W/m}^2$, $I_0 = 15{\cdot}10^5\,\text{W/m}^2$, $I_0 = 20{\cdot}10^5\,\text{W/m}^2$ and $I_0 = 25{\cdot}10^5\,\text{W/m}^2$ with the same exposure time 120 s. In Fig. 6, the temperature history at the point $(0.0002\,\text{m}, 0.002\,\text{m})$ for all variants of computations is shown. For high laser powers, the temperature at this point exceeds

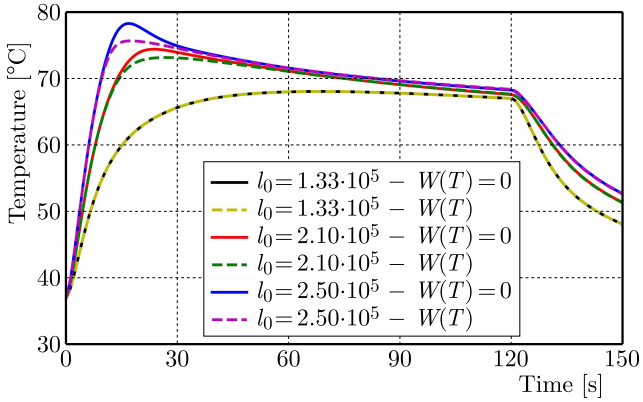

Fig. 5. Temperature history for different laser powers with a zero and non-zero $W(T)$ function – point $(0.0002\,\mathrm{m}, 0.0002\,\mathrm{m})$, exposure time 120 s

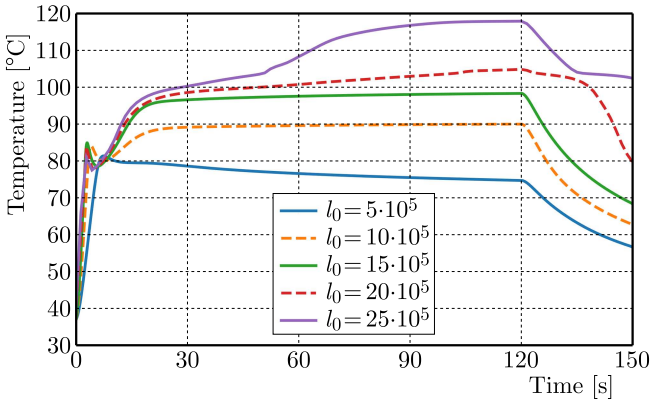

Fig. 6. Temperature history for different laser powers – exposure time 120 s – point $(0.0002\,\mathrm{m}, 0.0002\,\mathrm{m})$

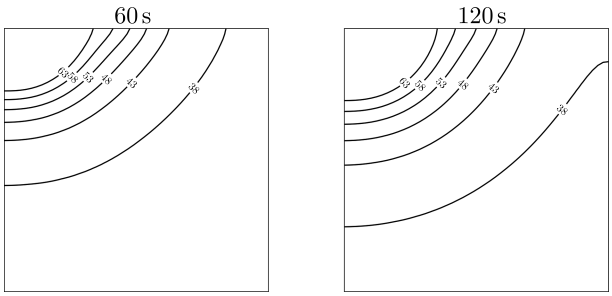

Fig. 7. Temperature distribution after 60 s and 120 s, $I_0 = 25 \cdot 10^5\,\mathrm{W/m^2}$, exposure time 120 s

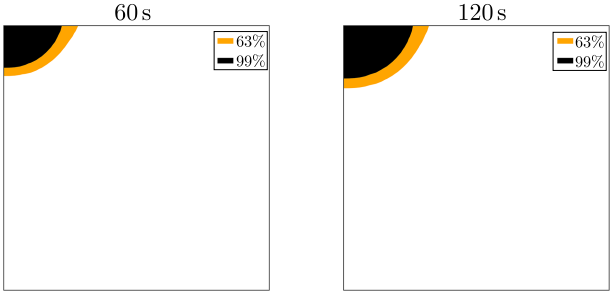

Fig. 8. Arrhenius integral distribution after 60 s and 120 s, $I_0 = 25 \cdot 10^5\,\mathrm{W/m^2}$, exposure time 120 s

100°C, and the water contained in the tissue undergoes an intensive evaporation process. In Figs. 7 and 8, the temperature and Arrhenius integral distributions in the domain for the time 60 s and 120 s are shown. It is clearly visible that for the laser power $I_0 = 25 \cdot 10^5\,\mathrm{W/m^2}$, the region of complete tissue destruction is quite large (e.g. for 60 s) and increases as the heating process continues (e.g. for 120 s).

5. Conclusions

The presented method of modeling of interactions of laser with biological tissue is based on the dual-phase lag equation coupled with the optical diffusion equation. The equations considered take into account thermophysical parameters of tissue that change with temperature and the optical parameters of biological tissue that change with the Arrhenius integral. It has been shown that in the modeling of high-temperature hyperthermia, it is important to use variable optical parameters of the tissue. The use of constant optical parameters leads to excessive temperatures, which may result in an inaccurate assessment of the degree of damage to biological tissues, which may consequently affect the correct planning of artificial hyperthermia treatments. An important element of the computations is the analysis of water percentage in the tissue. Taking into account the function $W(T)$ allows for modeling of the evaporation process. The evaporation of water and other fluids from the tissue significantly affects the obtained temperature values and, consequently, the size of the estimated domain of damage.

Acknowledgment

The research was funded from financial resources from the statutory subsidy of the Faculty of Mechanical Engineering, Silesian University of Technology.

References

1. Abraham J., Sparrow E., 2007, A thermal-ablation bioheat model including liquid-to-vapor phase change, pressure and necrosis-dependent perfusion, and moisture-dependent properties, *International Journal of Heat and Mass Transfer*, **50**, 13-14, 2537-2544
2. Ashley J., Welch M.A.J., Gemert M.J.C. [Edit.], 1995, *Optical-Thermal Response of Laser-Irradiated Tissue*, Plenum Press, New York
3. Barnoon P., Bakhshandehfard F., 2021, Thermal management in a biological tissue in order to destroy tissue under local heating process, *Case Studies in Thermal Engineering*, **26**, ID 101105
4. Dombrovsky L.A., Baillis D., 2010, *Thermal Radiation in Disperse Systems: An Engineering Approach*, Begell House, New York
5. Dombrovsky L.A., Timchenko V., Jackson M., 2012, Indirect heating strategy of laser induced hyperthermia: an advanced thermal model, *International Journal of Heat and Mass Transfer*, **55**, 17-18, 4688-4700
6. Ellebrecht D.B., Theisen-Kunde D., Kuempers Ch., Keck T., Kleemann M., Wolken H., 2018, Analysis of laparoscopic laser liver resection in standardized porcine model, *Surgical Endoscopy*, **32**, 4966-4972
7. Fasano A.,Hömberg D, Naumov D., 2010, On a mathematical model for laser-induced thermotherapy, *Applied Mathematical Modelling*, **34**, 12, 3831-3840
8. Foster J., Hodder S.G., Lloyd A.B., Havenith G., 2020, Individual responses to heat stress: implications for hyperthermia and physical work capacity, *Frontiers in Physiology*, **11**, 28 pp
9. Giglio M.C., Logghe B., Garofalo E., Tomassini F., Vanlander A., *et al.*, 2020, Laparoscopic versus open thermal ablation of colorectal liver metastases: a propensity score-based analysis of local control of the ablated tumors, *Annals of Surgical Oncology*, **27**, 2370-2380

10. Jacques S.L., Pogue B.W., 2008, Tutorial on diffuse light transport, *Journal of Biomedical Optics*, **13**, 4, 1-19

11. Jasiński M., Majchrzak E., Turchan Ł., 2016, Numerical analysis of the interactions between laser and soft tissues using generalized dual-phase lag model, *Applied Mathematical Modeling*, **40**, 2, 750-762

12. Jaunich M., Raje S., Kim K., Mitra K., Guo Z., 2008, Bio-heat transfer analysis during short--pulse laser irradiation of tissues, *International Journal of Heat and Mass Transfer*, **51**, 5511-5521

13. Kim B.M., Jacques S.L., Rastegar S., Thomsen S., Motamedi M., 1996, Nonlinear finite--element analysis of the role of dynamic changes in blood perfusion and optical properties in laser coagulation of tissue, *IEEE Journal of Selected Topics in Quantum Electronics*, **2**, 4, 922-933

14. Kim K., Guo Z., 2007, Multi-time-scale heat transfer modeling of turbid tissues exposed to short-pulsed irradiations, *Computer Methods and Programs in Biomedicine*, **86**, 112-123

15. Lopresto V., Argentieri A., Pinto R., Cavagnaro M., 2019, Temperature dependence of thermal properties of ex vivo liver tissue up to ablative temperatures, *Physics in Medicine and Biology*, **64**, 10, 13 pp

16. Majchrzak E., Stryczyński M., 2022, Numerical analysis of biological tissue heating using the dual-phase lag equation with temperature-dependent parameters, *Journal of Applied Mathematics and Computational Mechanics*, **21**, 3, 85-98

17. Majchrzak E., Turchan Ł., Jasiński M., 2019, Identification of laser intensity assuring the destruction of target region of biological tissue using the gradient method and generalized dual-phase lag equation, *Iranian Journal of Science and Technology – Transactions of Mechanical Engineering*, **43**, 3, 539-548

18. Mochnacki B., Majchrzak E., 2007, Identification of macro and micro parameters in solidification model, *Bulletin of the Polish Academy of Sciences, Technical Sciences*, **55**, 1, 107-113

19. Niemz M.H., 2007, *Laser-Tissue Interaction: Fundamentals and Applications*, Springer-Verlag, Berlin, Heidelberg, New York

20. Szasz A., Szasz N., Szasz O., 2011, *Oncothermia: Principles and Practices*, Springer

21. Tzou D.Y., 1995, A unified field approach for heat conduction from macro- to micro-scales, *Journal of Heat Transfer*, **117**, 1, 8-16

22. Yang D., Converse M.C., Mahvi D.M., Webster J.G., 2007, Expanding the bioheat equation to include tissue internal water evaporation during heating, *IEEE Transactions on Biomedical Engineering*, **54**, 8, 1382-1388

23. Zhou J., Zhang Y., Chen J. K., 2009, An axisymmetric dual-phase lag bio-heat model for laser heating of living tissues, *International Journal of Thermal Sciences*, **48**, 8, 1477-1485

Manuscript received November 8, 2023; accepted for print January 15, 2024